Available online at www.sciencedirect.com
ScienceDirect
Fire Safety Journal 42 (2007) 150–160
FIRE SAFETY JOURNAL
www.elsevier.com/locate/firesaf

A computational and experimental study of ultra fine water mist as a total flooding agent

K.C. Adiga[a,*], Robert F. Hatcher Jr[a], Ronald S. Sheinson[b], Frederick W. Williams[b], Scott Ayers[c,1]

[a]*NanoMist Systems, LLC, 151 Osigian Blvd, Suite 199, Warner Robins, GA 31088, USA*
[b]*The Navy Technology Center for Safety and Survivability, Chemistry Division, Naval Research Laboratory, Washington, DC 20375-5320, USA*
[c]*Geo-Centers, Inc., 5813 Bayside Rd Building 307, Chesapeake Beach, MD 20732, USA*

Received 27 February 2006; received in revised form 10 August 2006; accepted 21 August 2006
Available online 1 December 2006

Abstract

Computational fluid dynamics (CFD) calculations were carried out to design total flooding fire tests in a 28 m^3 compartment for an ultra fine water mist ($<10\,\mu m$). The exit momentum of the mist produced by a proprietary ultrasonic generator technology was extremely low with a mist discharge velocity below 1 m/s. The mist was discharged with multiple floor outlets equally spaced around the centrally located 120 kW pool-like gas fire. The transport of mist and its interaction with the fire was simulated by Fluent, a commercial CFD model. Lagrangian Discrete Phase Model (DPM) was used for droplets. Simulation predicted extinguishment within 10 s with a mist delivery rate of 1 l/min. However, in total flooding fire tests conducted, extinction times were more than 5 min. Additional computations approximating the ultra fine mist (UFM) as a dense gas agreed well with the observed transport timescales of minutes indicating that UFM behaves like a gas. Further, the mist–fire interaction needs a multi-phase Euler–Euler approach with a droplet vaporization model.

Keywords: CFD modeling; Total flooding; Ultra fine water mist; Discrete Phase Model; Dense gaseous species model; Gas-like mist; Pseudo-gas mist

1. Introduction

Recent research indicates that a very low momentum gas-like ultra fine water mist ($<10\,\mu m$) system [1–6] has great potential in fire suppression applications including total and local flooding. The fine water mist is environmentally friendly with no toxic gas evolution, is easily available, and is a permanent solution. Droplets smaller than 10 μm begin to exhibit gas-like behavior with a superior ability to diffuse around obstructions without significant loss of mist due to plating and deposition. Prior studies [3,6] also demonstrated the ability of ultra fine mist (UFM) to overcome obstructions in a sub-floor as well as in total flooding tests. Ndubizu et al. have shown the superiority of ultafine mist in extinguishing boundary layer flames in wind tunnel experiments [7]. The UFM behaves like a clean gas agent and rapidly absorbs heat because of the large surface area and high vaporization rate of micron-sized mist droplets. The UFM is generated using a patented ultrasonic atomization device with a new process technology for aerosolization, extraction, and classification of fine droplets. The proprietary technology has the trademark, NanoMist® [8,9]. This ambient pressure atomization produces droplets less than 10 μm with a relatively narrow droplet-size distribution [3,10]. The conventional pressure atomization generally yields a broad droplet-size distribution. Because the mist is not generated using traditional nozzle technology, it presents a different challenge in meeting target fire suppression technology applications.

The ultra fine water mist generated by NanoMist® in this study behaves like a dense gas [1–6] unlike streaming

*Corresponding author. Tel.: +1 478 953 2709; fax: +1 478 953 3169.
E-mail address: kcadiga@nanomist.com (K.C. Adiga).
[1]Current address: Kidde Aerospace, 4200 Airport Blvd NW, Wilson, NC 27896, USA.

0379-7112/$ - see front matter © 2006 Elsevier Ltd. All rights reserved.
doi:10.1016/j.firesaf.2006.08.010

regular nozzle-based pressure atomized mist [11–16]. Proper engineering of the mist discharge and transport into the firebase or flame reaction zone is critical to the success of the UFM technology. For gas-like UFM, the extent of mist entrainment into the firebase depends on the coupled behaviors of the fire-induced flow-field and the mist flow rather than one-way streaming flow of pressurized mist from the nozzle. The rapid cooling of the fire reaction zone occurs due to the large surface area of UFM droplets. The rate and amount of mist entering the firebase are key factors in the suppression behavior of UFM.

Computational fluid dynamics (CFD) studies in the past have focused on the interaction of water mist with fires [17,18]. The emphasis of the present study is on designing total flooding fire test parameters to evaluate the performance of a proprietary UFM provided by NanoMist Systems, LLC. FLUENT, a commercial CFD program, was used [19] with relatively simple sub-model elements. Since the objective was to model UFM transport and entrainment of mist into the firebase, a simple pool-like hot gas fire [20,21] was used. Combustion chemistry and radiation sub-models were not activated in this study. As the computationally cost-effective approach, the Discrete Phase Model (DPM) of CFD was used to simulate the mist transport and entrainment of mist into the firebase and the cooling of the fire by droplet vaporization. Additional simulations were carried out treating UFM as a dense gas using the species transport model.

The test parameters evaluated by CFD simulations were used as guidelines for field-testing at the Chesapeake Bay Detachment (CBD) facility of the Naval Research Laboratory (NRL). The objective was to compare the field test results with the CFD model and to determine possible limitations of the current systems. The other objective was to compare oxygen measurement techniques to help understand the suppression dynamics of very fine water mist. This increased understanding can lead to significant technological improvements.

2. CFD simulation

2.1. Geometry and outline

The geometry and mesh were created using the Gambit preprocessor provided by the Fluent CFD package. The fire compartment was $3 \times 3 \times 3$ m. The floor area of 3×3 m was divided into 9 equal zones of $1\,m^2$. The central zone contained a 0.3-m diameter pool-like gas fire. Eight mist outlets were installed at the center of each of the eight surrounding zones. This layout is shown in Fig. 1. The total mass flow was equally divided amongst these outlets. The flux density was calculated by dividing the floor area of $9\,m^2$ by the flow rate. The outlets were given fan boundary conditions in order to simulate a required mass flow of air of 0.0125 kg/s in each fan outlet. The mist droplets were later injected from this surface. The diameter of the mist

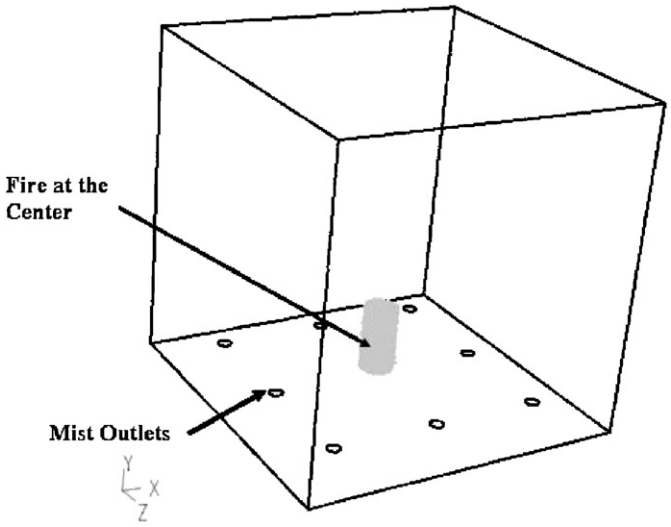

Fig. 1. Configuration of NanoMist discharge outlets on the floor of test compartment.

outlet tube was 0.10 m. The geometry was meshed using 72,000 tetrahedral cells.

Fluent CFD [19] with a κ–ε turbulence model was used to simulate a compartment fire with a set of predecided deployment configurations. The Fluent DPM was used to simulate the distribution of UFM, the mist entrainment into the fire, and the subsequent droplet vaporization resulting in the fire-cooling process. The Lagrangian scheme treats the particle phase as the discrete phase and the fluid phase as a carrier phase in an Eulerian frame. Trajectories of individual particles can be calculated by the balancing forces acting on them. In the Lagrangian particle tracking approach, particle phase and fluid phase interactions are accounted for by iteratively updating the fields at predetermined intervals. The drying particle trajectories influenced by turbulence are predicted by the discrete phase random walk tracking approach. The details are available in Ref. [19] (Fluent Manual). A pool-like gas fire [20,21] model without fire chemistry and radiation was used to generate fire as well as mist–fire interaction.

3. Results and discussion of CFD simulation

3.1. Fire simulation

The fire was simulated by a volumetric heat release source within a cylindrical gas volume of 0.3 m in diameter and 0.6 m high as shown in Fig. 1. The heat release rate input was varied to give a 120 kW fire with peak temperatures 900–1000 °C. This peak temperature compares well with the experimental turbulent heptane pool fires [11]. Fig. 2 shows the pool-like fire located at the center of the compartment floor 2 s into the test. The time-dependent fire simulations were carried out to 15 s in order to capture the unsteady behavior of the fire temperature. The transient trend observed provides a calibration curve

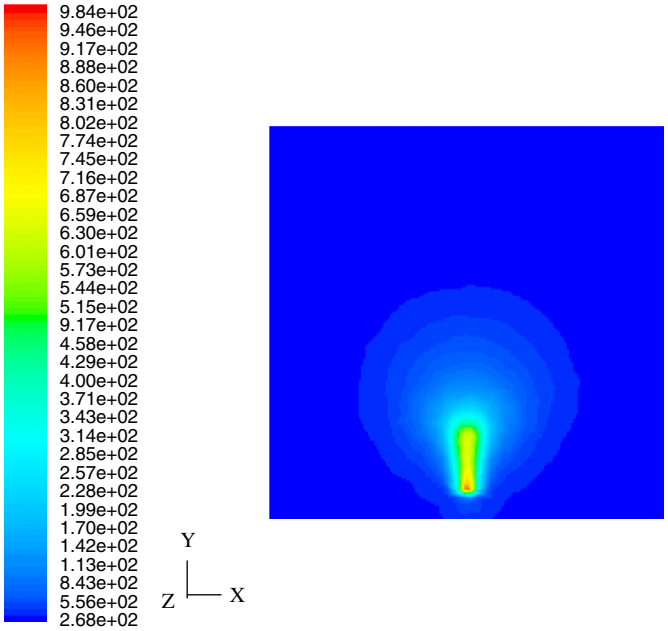

Fig. 2. Temperature (°C) contours of fire at $t = 2$ s. The peak temperature is 984 °C.

for the fire behavior before the mist is deployed into the room.

3.2. Mist deployment and mist–fire interaction

Monodisperse droplets of 10-μm diameter were introduced through 8 mist outlets with fan boundary conditions at the outlet surfaces. The injection mass flow at each outlet was 0.002 kg/s giving a total mist discharge of 0.017 kg/s. This provides volumetric flow of 1 l/min of mist discharge through outlets on the floor surrounding the central fire. Based on the mass of air through the fan of 0.0125 kg/s, the mass fraction at each mist outlet will be approximately 0.14. The injection of UFM was initiated after a preburn period of 2 s. Fig. 3A shows the velocity vectors inside the compartment with the fire located at the center. The flow close to the firebase is relatively weak except at mist outlets. This is an important computational result to notice because the dispersion and the fill rate of mist at the base of the compartment will be limited to this transport velocity. If a dense gas were to be discharged at these outlets, the dispersion time for the gas to reach the fire location would be a function of this background flow-field.

At the base of the compartment, the fire entrains the air into the base as shown by a close-up in Fig. 3B. If mist is positioned at these locations with a suitable flow condition, it will be entrained into the firebase; otherwise, droplets fall out or sweep across the firesides downstream. This observation is supported by the entrainment of inert droplets into the firebase as shown by the calculated inert droplet trajectories in Fig. 4A. Fig. 4B shows trajectories of droplets with the vaporization process activated in the DPM model. The numerical simulation supports the concept of self-entrainment of mist into the firebase as shown by experiments in earlier work [1–2].

Local flooding experiments on a 0.3 m heptane pool fire showed self-entrainment behavior, as shown in Fig. 5, when the mist cloud surrounds the fire. The mist surrounding the firebase has extremely low momentum and is quickly pulled into the firebase; the fire goes out within 5–10 s. If the mist is transported near the firebase with a low momentum and a matching flow condition, the entrainment will be efficient and the extinction will be quick. The extinction of fire in a total flooding scenario may not be reproduced with this local flooding test since mist should be transported to the firebase. This transport is mainly by diffusion since mist injection velocity is <1 m/s, and the momentum is extremely low. The convection transport is very weak in this scenario.

The extent of entrainment of mist into the firebase in the present simulation can be inferred from the vaporized mass fraction of water inside the fire geometry. Fig. 6 shows the water vapor mass fraction contour at time $t = 10$ s. The maximum vapor mass fraction of 0.19 is seen at the firebase. Based upon the latent heat absorption by the mist, this region of the fire shows a considerable temperature drop. The time-dependent cooling of fire upon the injection of mist is shown in Fig. 7 by centerline peak temperatures. Within about 10 s, the fire peak temperature cools from 984 to about 770 °C. The fire cooling continues, indicating the tendency to go out. These results were obtained at a water mist flow of 1 l/min.

The drop in centerline peak temperature of 100 °C or more was considered the extinction criterion in this work. When temperature drops below this limit, the fire cools continuously and goes out. The extinguishment time of close to 10 s seems reasonable when compared with local flooding tests conducted on heptane pool fires as shown in Fig. 5. However, in the context of total flooding in a room, the transport of mist to the firebase plays a key factor in limiting the mist concentration at and near the firebase, unlike in a local flooding application. The total flooding experiments described in the next sections will provide extinction time scales and give guidance as to how the DPM can be used as an engineering tool for UFM flooding.

4. Total flooding experiments

4.1. Compartment and test layout

The total flooding experiments were performed at the NRL, Chesapeake Bay Detachment, MD. The test was conducted in a 28 m^3 cubic, steel walled compartment with a standard Navy ventilation system providing one air exchange every 4 min. The supply vent was located near the ceiling while the exhaust vents were split two-thirds low and one-third high. The compartment resembled the simulated compartment as closely as possible. NanoMist Systems, LLC, supplied the mist generation units used

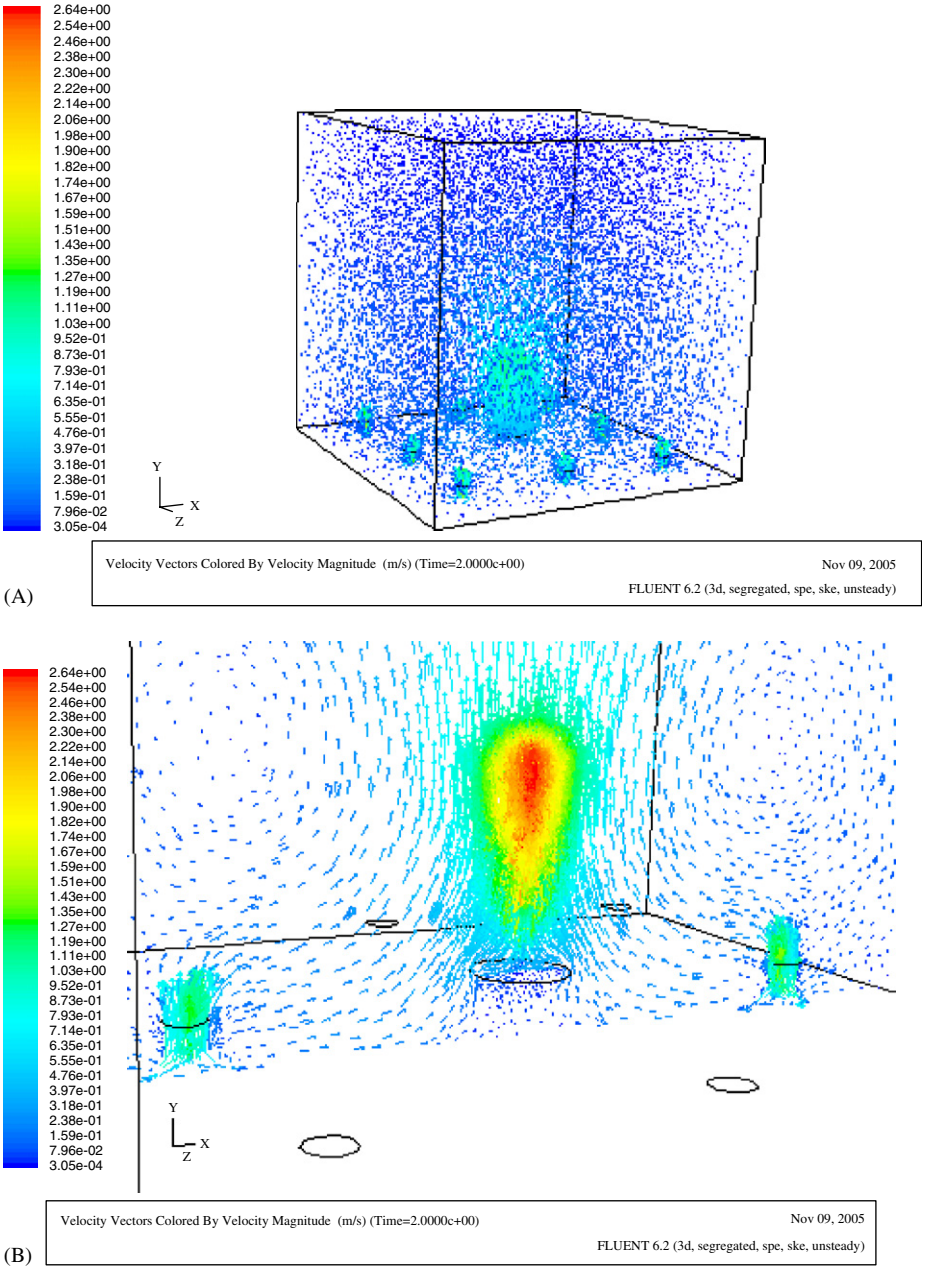

Fig. 3. (A) Velocity vectors (m/s) inside the compartment and (B) velocity vectors (m/s) near the firebase—a close-up view.

[1,8]. The power required per unit could be set to either 110 V at 12 A or 220 V at 6 A. Air was supplied to each mist unit through an inlet fan. Water was introduced at the base of the mist unit from a reservoir and excess water re-circulated into the reservoir. This system maintained the constant water level needed for efficient mist generation. Four-inch PVC pipes were used to duct the mist from the top of the mist unit to the upward vertical outlets on the deck. Water that "condensed" out in the ducts was collected and measured.

The instrumentation layout detailed included a thermocouple tree with five thermocouples at 0.76, 1.14, 1.52, 1.90, and 2.52 m off the deck to characterize the compartment temperatures. The test layout is shown in Fig. 8. As seen in Fig. 8, only six mist outlets were used in experiments as opposed to eight in the CFD model. Two thermocouples were placed above the fire pan to help determine extinguishment time. Two gas sampling lines were located in the compartment, withdrawing air samples from one high and one low location (heights indicated in Fig. 8). A paramagnetic oxygen balance and an IR analyzer measured oxygen and carbon dioxide concentrations, respectively in each sampling line. A heated zirconium oxide electrochemical sensor and a tunable diode laser in situ multi-pass absorption gas cell were also used to measure oxygen near the lower gas sampling line (heights indicated in Fig. 8). Visible and IR video cameras were used to observe the fire.

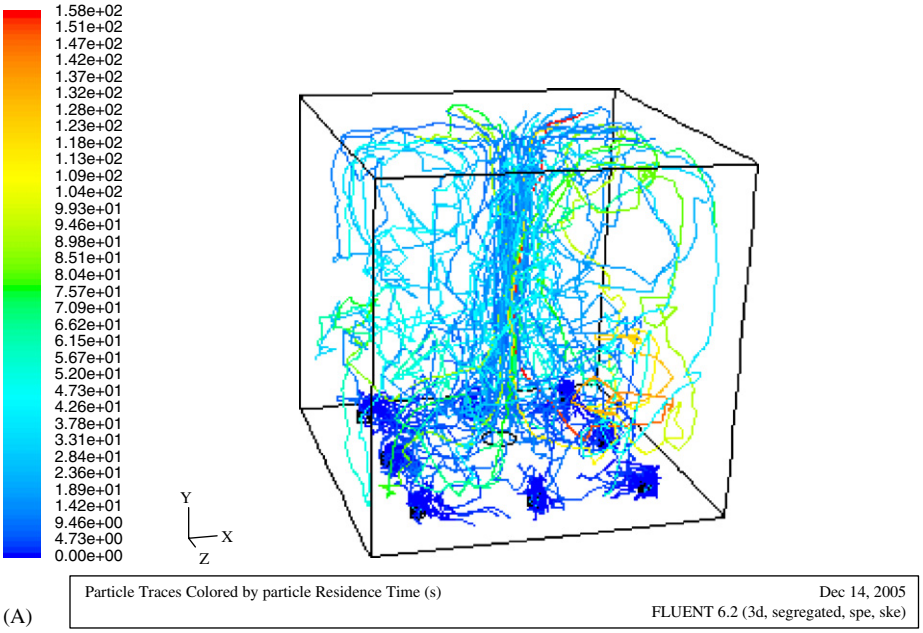

Fig. 4. (A) Stochastic droplet trajectories of inert droplets and (B) droplet trajectories with vaporization.

4.2. Oxygen measurement

Knowing the actual oxygen concentration near the fire is critical for understanding extinction. Three oxygen measurements were made of the fire-entrained air in order to compare the different measurement techniques. The paramagnetic oxygen analyzer (using gas withdrawn from the test compartment) requires almost all of the water to be removed from the gas stream for proper operation. A dry oxygen molar concentration measurement is then produced. The zirconium oxide sensor, in contrast, operates above 600 °C; all liquid water (mist) is vaporized. The measurement is thus a wet oxygen molar concentration measurement (fully diluted by water vapor). The Tunable Diode Laser Absorption Spectroscopy (TDLAS) measures actual oxygen molar concentration directly, without the influence of liquid water. The TDLAS oxygen measurement is a developing technology and is presented elsewhere [10]. If the difference between the wet and dry oxygen measurements is due to water only, the two measurements can be used to infer the water mass concentration as follows:

$$m_{H_2O} = \frac{MW_{H_2O}}{\sum MW_i x_i^{wet}} \left(1 - \frac{x_{O_2}^{wet}}{x_{O_2}^{dry}}\right). \quad (1)$$

Fig. 5. Self-entrainment of ultra fine mist at the base of heptane pool fire (0.3 m) in a local flooding scenario.

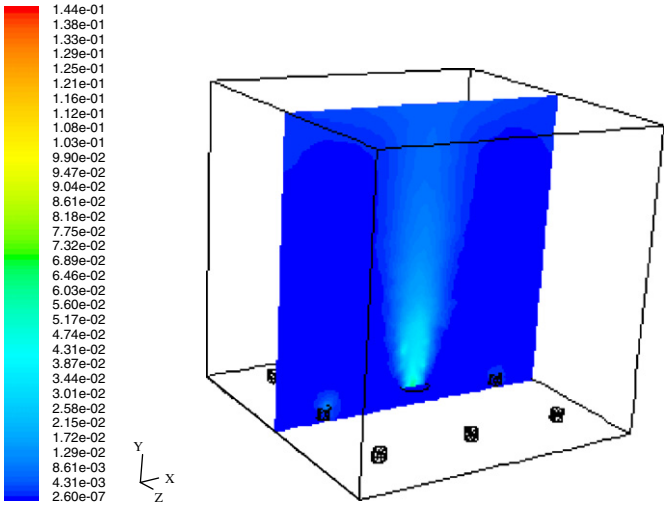

Fig. 6. Water vapor mass fraction at $t = 10$ s. The peak value of mass fraction is 0.19.

Since the carbon dioxide concentration by IR is also a dry gas analysis, a correction needed to be applied to determine the concentration of carbon dioxide with respect to water:

$$x_{CO_2}^{wet} = x_{CO_2}^{dry} \frac{x_{O_2}^{wet}}{x_{O_2}^{dry}}, \quad (2)$$

where m_{H_2O} is the water mass concentration; MW_{H_2O} is the molecular weight of water; and $MW_i x_i^{wet}$ is the product of molecular weight and molar concentration of either water, oxygen, carbon dioxide, or nitrogen; $x_{O_2}^{wet}$ is the wet molar concentration measurement of oxygen; $x_{O_2}^{dry}$ is the dry molar concentration measurement of oxygen; and $x_{CO_2}^{dry}$ is the dry molar concentration measurement of carbon dioxide.

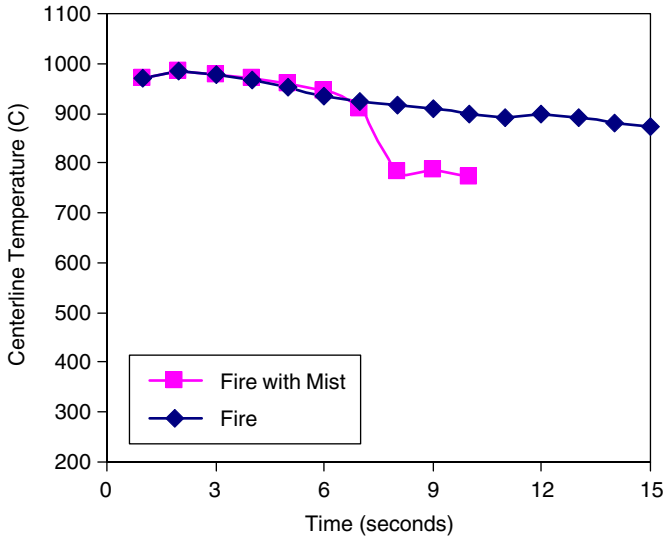

Fig. 7. Peak centerline temperatures for baseline (no mist) and after mist injection.

4.3. Test variables

The test plan initially called for four mist units each producing 250 ml/min to be used with a 120 kW heptane fire near the deck. Varying mist concentration was accomplished by varying the number of mist units used—four, five, or six. The second variable was the fire size and fuel. In addition to the 120 kW heptane fire, a 5 kW heptane fire (five 2.5 cm heptane tell-tales placed in the dry fire pan), and a 70 kW methanol fire were used. The third variable was the addition of a simple obstruction/partial wall to challenge the mist transport. Table 1 shows the 12 scenarios tested.

4.4. Test procedure

Table 2 shows the test sequence of events, the time referenced to the start of the data acquisition. The fire was manually ignited at 60 s. The compartment was then sealed at about 70 s. The mist units were activated and the ventilation was secured at 120 s. The fire was extinguished either by the mist or fuel consumption at time, T_x, after 120 s. The mist units were secured, and the ventilation was activated at time, T_y, after T_x.

At the completion of each test, the compartment was vented. Re-entry was made once the space was determined to be "gas-free" by a certified technician. The water loss in the recirculation system and the water condensed out in the ducting were measured to find a

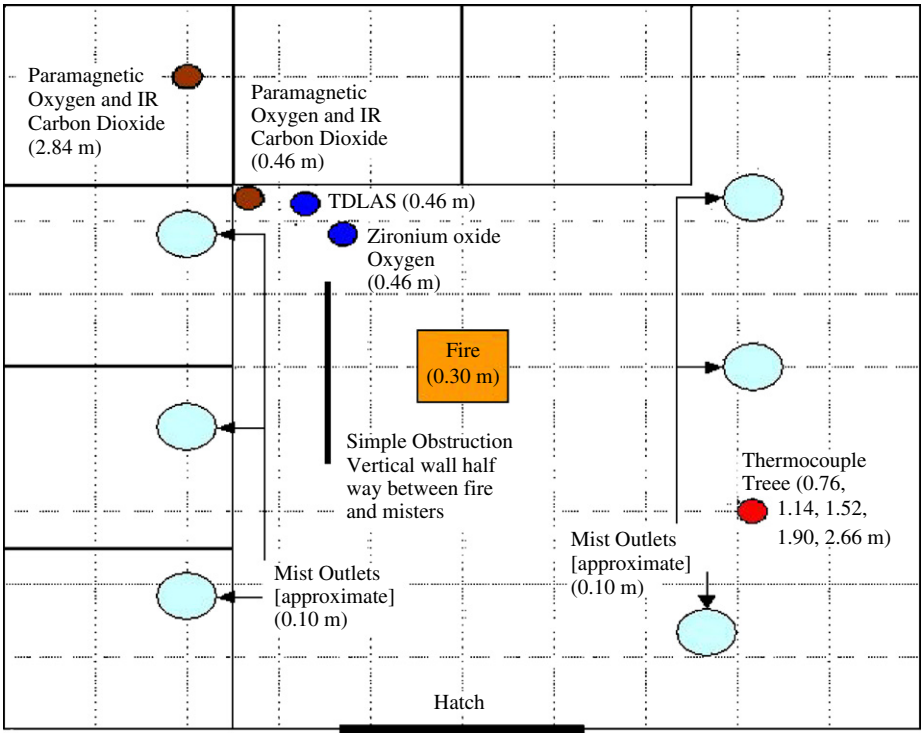

Fig. 8. Test layout of NRL–CBD compartment fire test scenario.

Table 1
Test Matrix

Fire size (kW) and fuel	Wall	Misters
No fire	—	6
No fire	—	5
No fire	—	4
120 heptane	—	None
5 heptane	—	None
70 methanol	—	None
120 heptane	—	6
5 heptane	—	6
120 heptane	—	5
120 heptane	—	4
120 heptane	Yes	6
70 methanol	—	6

Table 2
Test procedure

Time (s)	Event
0	Data acquisition start, test begins
60	Fire manually ignited
~70	Compartment door secured
120	Mist activated, ventilation secured
T_x	Fire extinguished
T_y	Mist secured, ventilation activated

total mist generation rate. The remaining fuel in the fire pan was also measured to reaffirm extinguishment by the mist.

5. Experimental results and discussion

5.1. Fire extinction time scales

Table 3 shows the extinguishment times for the test scenarios. The results clearly show that the extinguishment times are reproduced by the CFD computer simulation using the DPM model. The CFD simulation predicted extinguishment times within 10 s, while the tests took more than 5 min for extinguishment. The reasons for this anomaly will be discussed in the next section. As seen in Fig. 9, extinguishment time decreased with increased mist generation rate.

The total volume of mist delivered can be found by multiplying the mist generation rate by the extinguishment time. Fig. 10 highlights the results of using different number mist units, the simple obstruction, and the methanol fire. The simple obstruction showed increased liquid volume requirement due to distribution losses including the loss of mist droplets by deposition/plating on the obstruction plate. Compared to six-mist units, the four-mister configuration showed an increased volume requirement. The decreased number of misters reduced the number of outlets making the mist dispersion less efficient. In addition, the reduced mist generation by 4-misters allows time for the continuing fire generated energy to counteract more mist. The methanol pool fire took significantly higher amount of water for suppression.

The lack of soot in methanol fires minimizes radiation heat losses, requiring more energy abstraction (and thus

Table 3
Total flooding ultra fine water mist (NanoMist®) results

Fire size (kW) and fuel	Wall	Mist units	Extinguishment time (s)	Mist rate (l/min)	Total volume (l)
120 heptane[a]	—	6	283	0.64	3.02
120 heptane	—	6	301	0.65	3.26
120 heptane		6	306	0.66	3.37
120 heptane	—	4	357	0.56	3.33
120 heptane	—	4	391	0.61	3.98
120 heptane	Yes	6	329	0.70	3.84
70 methanol[b]	—	6	521	0.62	5.38

[a]120 kW heptane fire would burn for more than 480 s.
[b]70 kW methanol fire would burn for more than 660 s.

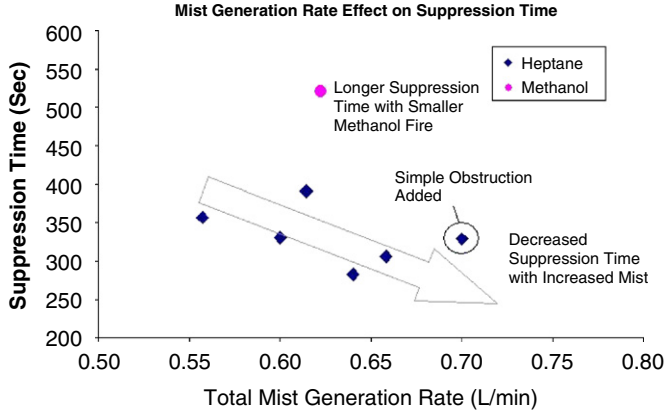

Fig. 9. The extinguishment times as a function of total mist generation rate.

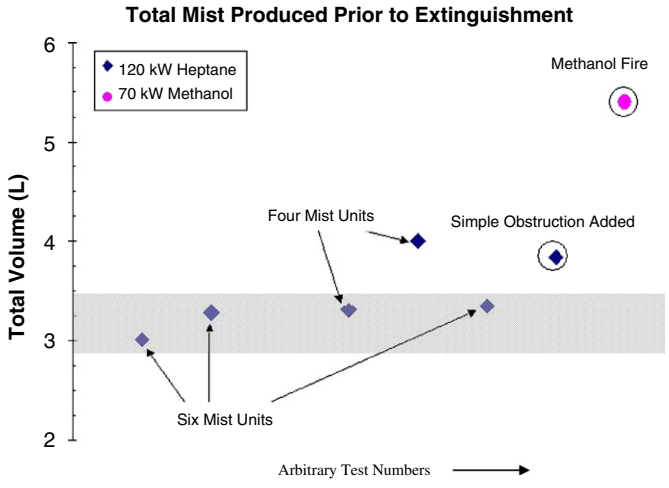

Fig. 10. The total volume of mist produced before extinguishment for the tests.

more agent) to accomplish extinction. Methanol, with a lower oxygen index compared with heptane, is relatively less sensitive to the oxygen displacement mechanism by the expanding steam generated by the mist. The cup burner extinction for several agents including the chemical catalytic halon 1301–CF_3Br, chemically scavenging 1,1,1,2,3,3,3-heptafluoropropane, and physical agents N_2 and CF_4 show a larger amount of agent requirement for methanol as compared to heptane [22]. The suppression differential between methanol and heptane is very large for halon 1301(>2x). Methanol also requires greater agent concentrations for HFC-227ea, N_2, and CF_4 (1.3x, 1.4x) as compared to heptane. These work primarily by physical mechanisms. It is to be expected that water mist—a physical suppressant—would behave very similar to the cited physical agents.

5.2. Mist concentration results

The average water mist throughput was calculated from measuring the recirculation water volume consumption in the tests. With six mist units, the average value was found to be 0.66 l/min. This is well below the value of 1.0/min used in the CFD computer model. The carrier gas flow rate was measured after the test series at 360 l/min per mist unit or 2160 l total. The resulting mass concentration of water at the mist outlet was therefore ~20%. Fig. 11 compares the water mass concentration found from Eq. (1) in three test scenarios: mist only; a 120 kW heptane fire and 5.5 min of mist—the mist stopped at 5.5 min when fire was extinguished; and a 120 kW heptane fire and 10 min of mist. The water concentrations under no fire versus fire conditions showed that the fires greatly reduced the water mist density at the sensor positions. The time delay in attaining the peak concentration of mist is related to transport process. This took several minutes. This observation of long transport time of several minutes will be simulated and demonstrated in the next section by an alternate CFD model approach using dense gas species analogue for ultra fine water mist. The water mass concentration begins to plateau and eventually reaches about 9%. This is less than half the concentration at the outlet of the mist units. The difference between the mist without fire and mist with fire is significant. The variations in water concentrations traces for two fires is due to statistical variations of turbulent fire field and mist interaction causing the depletion of mist. The mist depletion processes in the presence of fire shows a clear

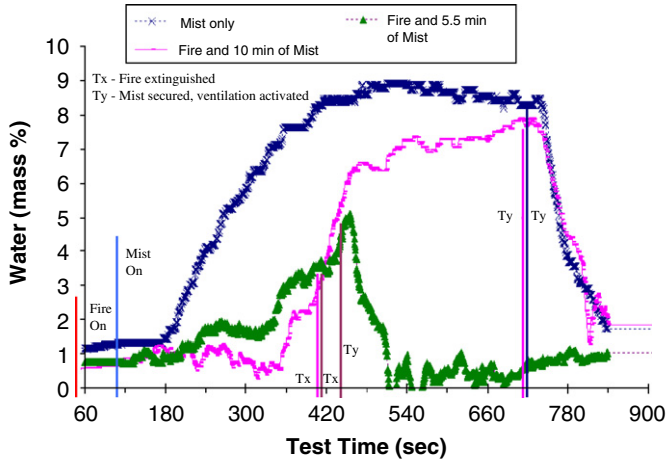

Fig. 11. Water mass concentration from several mist unit tests.

Fig. 12. A dense gas-like ultra fine water mist, NanoMist®, dispersion in a room.

indication of mist–fire interaction. This will be explored and quantified in future studies.

5.3. The physical appearance of mist dispersion

Fig. 12 shows ultra fine water mist dispersion inside the room. The mist behaves like a dense gas dispersing slowly from the discharge location. If the mist were deployed from the base upwards, it would start to fill the volume like a liquid, the extent of lateral dispersion depending on the flux density. The extent of vertical dispersion depends on outlet discharge velocity. The transport of mist resembles dense gas dispersion in an enclosure. This factor distinguishes ultra fine NanoMist® from regular or commercial mist. The nearly gas-like behavior of UFM may call for a gaseous species treatment. The next section describes the species transport approach to extremely fine mist and its relevance to UFM dispersion.

6. Dense gas model approach for NanoMist dispersion

In this treatment, the UFM was treated as a dense gaseous (DG) species. The bulk density of the dense gas with a water mass fraction of 0.14 is about 1.3 kg/m^3. The species DG has the transport properties of water vapor except for the density of 1.3 kg/m^3. DG was injected at the mist outlets with an identical carrier gas mass flow as in the case of mist. The mass fraction of DG was monitored at the fire location as a function of time with the identical pool-like gas fire at the center.

Similar to the entrainment of mist, the dense gas is entrained into the firebase. In order to compare the time scales of DG transport and the DPM model prediction of water vapor, the peak concentrations of DG and DPM inside the fire volume are plotted as functions of time in Fig. 13. As seen, the overall transport times of DPM concentrations are within 10 s while the dense gas model extends beyond a minute. The slow dispersion of DG demonstrates the vastly differing time scales of mist transport under weak convective flow at the firebase. This long transport time agrees qualitatively with the measured water concentration shown in Fig. 11. In fact, the experiments show several minutes to reach the peak concentration. Fig. 14 shows the dense gas mass fraction contours at various time intervals. The gas concentration at the central fire location increases with time as seen at the center of the floor where the fire is located. The time scales of mist transport to the fire location are in qualitative agreement with experimental extinction times. However, the dense gas model predictions did not include droplet vaporization and mist–fire interaction. As a result, a quantitative comparison of extinction time scales is beyond the scope of this work. The multi-phase Euler–Euler approach [19] with a droplet vaporization model is ideal for a quantitative modeling of the mist interaction with fire. More experimental studies by Abbud-Madrid et al. [23] and Ndubizu et al. [24] are now becoming available on

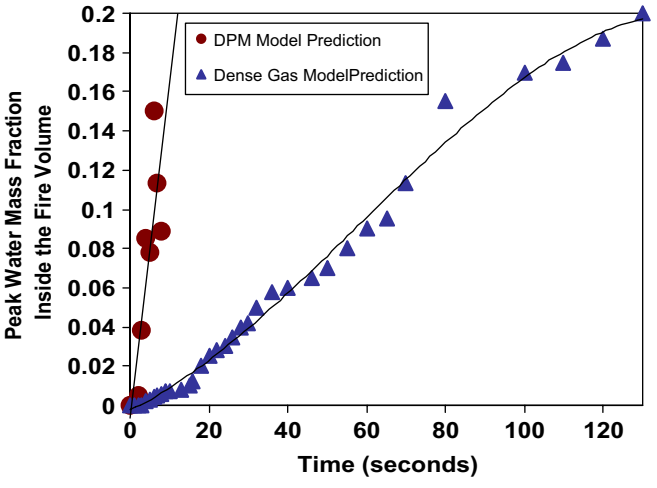

Fig. 13. Comparison of dense gas (DG) and DPM model concentration inside the fire volume as function of time.

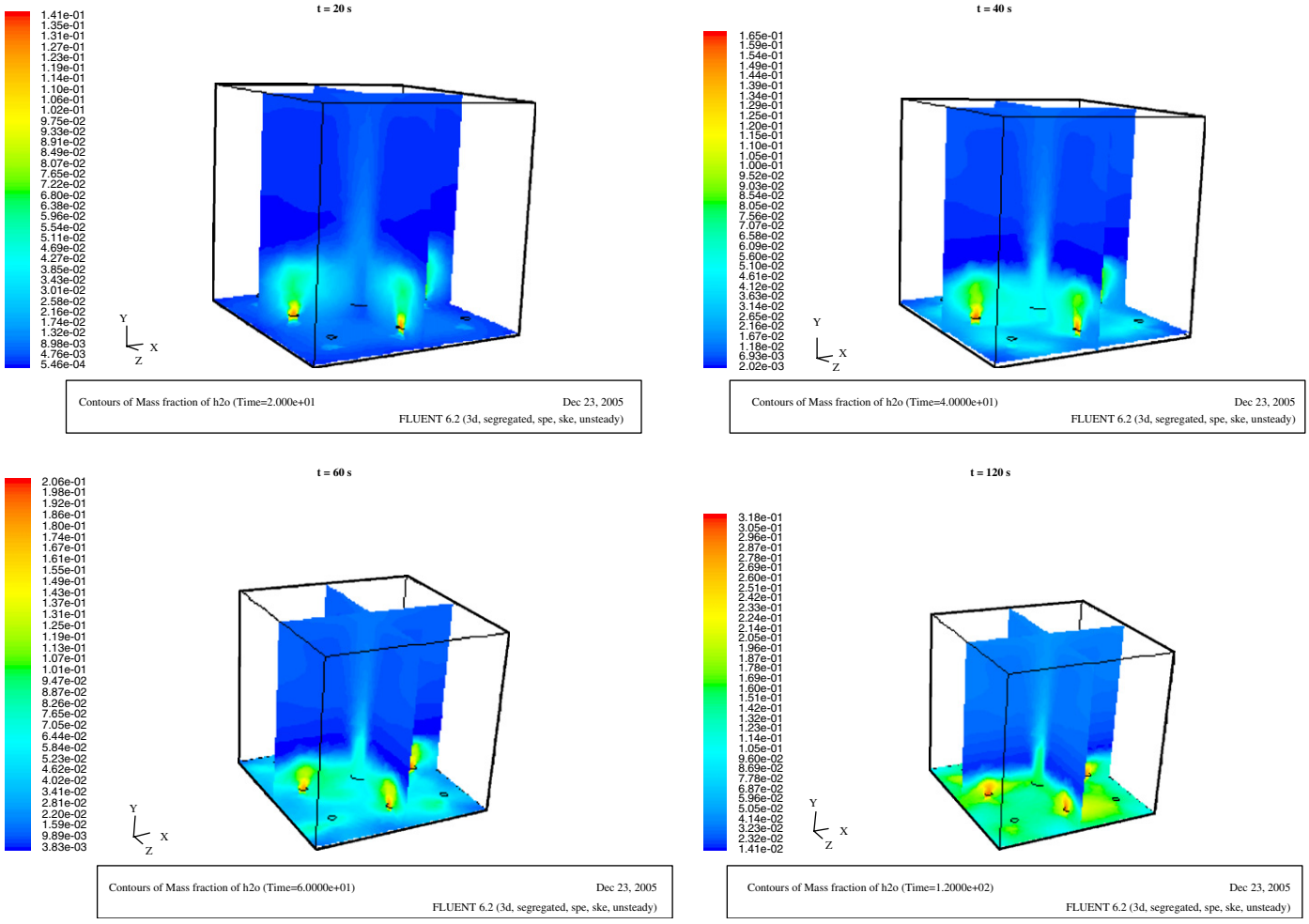

Fig. 14. Mass fraction contours of dense gas (DG) at various time intervals.

ultra fine water mist on other fire configurations such as Space Shuttle mid-deck locker mockup and cable fires in wind tunnel. Extending modeling to these scenarios should help establish the credibility of the above approach.

7. Conclusions

The ultra fine water mist was able to successfully extinguish all pool fires. The average extinguishment time of a 120 kW heptane fire was around 5 min with six mist units operating at a total of 0.66 l/min. The extinguishment time decreased with increasing mist injection rate. The addition of a simple obstruction required slightly more mist input to extinguish the fire. A 70 kW methanol fire was extinguished in approximately 8 min. The measured volume of water consumed by the misters differed from the predicted rates used in the computer model. The CFD simulations using DPM under predicted the extinction time scales. Transport of the low momentum UFM is a key consideration. The dense gas species approach to UFM showed a significant improvement in predicting the time-scales of the mist transport. With this approach, mist approaches the firebase in several minutes as observed in experiments.

The dense gas approach could be a robust engineering tool for estimating transport behavior of extremely low momentum UFM (diameter $<10\,\mu m$) for total flooding applications. However, the mist–fire interaction needs to be simulated using the multi-phase Euler–Euler approach with droplet vaporization.

Acknowledgments

The authors would like to recognize Clarence Whitehurst for his invaluable assistance in conducting the tests as well as James Fleming, Andrew Awtry, and Volker Ebert for their contributions to the oxygen measurements. This work was funded as part of the Office of Naval Research (ONR) Future Naval Capabilities (FNC), Advanced Damage Countermeasures (ADC) program. One of the authors (K.C. Adiga) thanks Fluent CFD support group for reviewing the CFD modeling approach.

References

[1] Adiga KC. Ultrafine water mist fire suppression technology. Fire Eng 2005;January:197–200.

[2] Adiga KC, Adiga R, Hatcher Jr RF. Self-entrainment of ultra fine water mist technology for new generation fire protection. In: Proceedings of workshop on fire suppression technologies, February 25–27, Mobile, Alabama, 2003.
[3] Adiga KC, Hatcher Jr RF, Forssell EW, Scheffey JL, DiNenno PJ, Back III GG, et al. False deck testing of Nanomist water mist systems. In: Proceedings halon options technical working conference, Albuquerque, New Mexico, 2005.
[4] Adiga KC, Williams FW. Ultra-fine water mist as a total flooding agent: a feasibility study. In: Proceedings halon options technical working conference, Albuquerque, New Mexico, 2004.
[5] Adiga KC. A CFD study of the effects of inlet droplet variables on water mist fire suppression efficiency. In: Proceedings of the 36th intersociety energy conversion engineering conference, vol. 1, Paper No. 2001-AT-77, 2001.
[6] Sheinson RS, Ayers S, Williams FW, Adiga KC, Hatcher Jr RF. Feasibility evaluation study of very fine water mist as a total flooding fire suppression agent for flammable liquid fires. In: Proceedings halon options technical working conference, Albuquerque, New Mexico, 2004.
[7] Ndubizu CC, Ananth R, Williams FW. Effects of air-borne water mist on the local burning rate of a PMMA plate in boundary layer combustion. In: Proceedings halon options technical working conference, Albuquerque, New Mexico, 2004.
[8] Adiga KC, Adiga R, Hatcher Jr RF. Method and device for production, extraction and delivery of mist with ultra fine droplets. US Patent 6,883,724, April 26, 2005.
[9] Adiga KC, Adiga R, Hatcher Jr RF. Fire suppression using water mist with ultra fine size droplets. US Patent 7,090,028, April 15, 2006.
[10] Awtry AR, Fleming JW, Ebert V. Simultaneous diode laser based *in situ* measurement of liquid water content and oxygen mole fraction in dense water mist environments. Opt Lett 2006;31(7):900–2.
[11] Ndubizu CC, Ananth R, Tatem PA. The effects of droplet size and injection orientation on water mist suppression of low and high boiling point liquid pool fires. Combust Sci Technol 2000;157:63–86.
[12] Liu Z, Kim AK. A review of water mist fire suppression technology: Part II Application studies. J Fire Protect Eng 2001;11:15–42.
[13] Heskestad G. Extinction of gas and liquid pool fires with water sprays. Fire Saf J 2003;38:301–17.
[14] Mawhinney JR, Dlugogorski BJ, Kim AK. A close look at the fire extinguishing properties of water mist. In: Proceedings of the fourth international symposium on fire safety science, IAFSS, 1994.
[15] Bill Jr. RG, Hansen RL, Richards K. Fine spray protection of shipboard engine rooms. Fire Saf J 1997;29:317–36.
[16] Back III GG, Beyler CL, Hansen RA. Quasi-steady-state model for predicting fire suppression in spaces protected by water mist systems. Fire Saf J 2000;35:327–62.
[17] Mawhinney R, Grandison A, Galea ER, Patel M, Ewer J. The development of a CFD based simulator for water mist suppression systems: the development of the fire sub model. Appl Fire Sci 2000;9:311–46.
[18] Prasad K, Li C, Kailasanath K. Optimizing water-mist injection characteristics for suppression of methane-air diffusion flames. In: Twenty-seventh symposium (international) on combustion, the Combustion Institute, 1998. p. 2847–55.
[19] Fluent user's guide vols. 1–4. Fluent Incorporated, Central Resource Park, 10 Cavendish Court, Lebanon, NH 03766, 1998–2004.
[20] Adiga KC, Ramaker DE, Tatem PA, Williams FW. Modeling pool-like gas flames of propane. Fire Saf J 1989;14:241–50.
[21] Adiga KC, Ramaker DE, Tatem PA, Williams FW. Numerical predictions for a simulated methane fire. Fire Saf J 1990;16:443–58.
[22] Zegers EJP, Williams BA, Fisher EM, Fleming JW, Sheinson RS. Suppression of nonpremixed flames by fluorinated ethanes and propanes. Combust Flame 2000;121:471–87.
[23] Abbud-Madrid A, Lewis SJ, Watson JD, McKinnon JT, Delplanque JP. Study of water mist suppression of electrical fires for spacecraft applications: normal-gravity results. In: Proceedings halon options technical working conference, Albuquerque, New Mexico, 2005.
[24] Ndubizu CC, Ananth R, Williams FW. Suppression of small electrical cable fires with Fine water mist. In: Proceedings of the fourth joint meeting of the US sections of the Combustion Institute, 22 March 2005, Philadelphia, PA.